UC Merced
UC Merced Previously Published Works

Title

Amyloid-associated activity contributes to the severity and toxicity of a prion phenotype

Permalink

https://escholarship.org/uc/item/66c7w9ws

Journal

Nature Communications, 5(1)

ISSN

2041-1723

Authors

Pezza, John A
Villali, Janice
Sindi, Suzanne S
et al.

Publication Date

2014

DOI

10.1038/ncomms5384

Peer reviewed

Amyloid-Associated Activity Contributes to the Severity and Toxicity of a Prion Phenotype

John A. Pezza[□,*], **Janice Villali**[□,^], **Suzanne S. Sindi**[+], and **Tricia R. Serio**[□,§,✉]

[□]Brown University, Department of Molecular Biology, Cell Biology and Biochemistry

[+]University of California, Merced, Applied Mathematics, School of Natural Sciences, 5200 Lake Rd., Merced, CA 95343

Abstract

The self-assembly of alternative conformations of normal proteins into amyloid aggregates has been implicated in both the acquisition of new functions and in the appearance and progression of disease. However, while these amyloidogenic pathways are linked to the emergence of new phenotypes, numerous studies have uncoupled the accumulation of aggregates from their biological consequences, revealing currently underappreciated complexity in the determination of these traits. Here, to explore the molecular basis of protein-only phenotypes, we focused on the *S. cerevisiae* Sup35/[*PSI*⁺] prion, which confers a translation termination defect and expression level-dependent toxicity in its amyloid form. Our studies reveal that aggregated Sup35 retains its normal function as a translation release factor. However, fluctuations in the composition and size of these complexes specifically alter the level of this aggregate-associated activity and thereby the severity and toxicity of the amyloid state. Thus, amyloid heterogeneity is a crucial contributor to protein-only phenotypes.

Introduction

Protein amyloids expand the range of phenotypes associated with a single genotype by serving as novel, self-replicating epigenetic determinants. In these cases, the heritable information is encoded by alternative protein conformations, which have the propensity to self-assemble into amyloid fibers. These complexes, in turn, associate with and incorporate other conformers of the same protein, effectively templating their refolding to the amyloidogenic state.[1,2] Through this process, the persistence, progression and transmission

[✉]To whom correspondence should be addressed: tserio@email.arizona.edu.
[*]present address, New England Biolabs, 240 County Rd., Ipswich, MA 01938
[^]present address, Brandeis University, Department of Biochemistry, 415 South St., Waltham, MA 02454
[§]present address, The University of Arizona, Department of Molecular and Cellular Biology, 1007 E. Lowell St., Tucson, AZ 85721

of a diverse array of phenotypes, ranging from neurodegenerative diseases in mammals to alternative gene expression states in yeast, becomes possible.[1]

The link between amyloid assembly and its biological consequences varies by protein, but two general models have emerged. In the first model, an amyloid-associated phenotype arises through the loss of a protein's normal function when it is incorporated into aggregates. The most well-studied examples of loss-of-function amyloid phenotypes are the *S. cerevisiae* prion proteins Ure2, Swi1, Cyc8, Mot3, Sfp1, and Sup35, whose amyloid states phenocopy deletions or mutations in these factors.[1] In the second model, an amyloid-associated phenotype arises through the gain of a novel function when a protein is incorporated into aggregates. The most widely studied gain-of-function phenotype is the toxicity associated with mammalian proteins implicated in neurodegenerative diseases, such as the prion protein (PrP) in Creutzfeldt-Jakob and mad cow diseases, Aβ in Alzheimer's Disease, and huntingtin in Huntington's Disease. However, gain-of-function beneficial traits, such as hormone storage, biofilm formation, organelle biogenesis, and long-term memory are also associated with the assembly of other proteins into amyloid.[1,3–5]

Regardless of the model, the protein-based phenotypes were originally believed to emerge once the amyloid accumulated beyond the threshold required to impact normal physiology. However, studies in multiple systems have uncoupled amyloid accumulation from its phenotypic effects. In mammals, pathogenesis correlates poorly with the accumulation of ataxin-1[6] or huntingtin[7] inclusions or protease-resistant PrP,[8–10] hallmarks of the amyloid state. Modulation of chaperone expression ameliorates toxicity of polyglutamine-expanded proteins in *Drosophila* without impacting their accumulation in aggregates.[11–13] And finally in *C. elegans*, depletion of the insulin/insulin-like growth factor-1 receptor DAF-2 suppresses $A\beta_{1-42}$ toxicity while promoting the accumulation of high molecular weight aggregates of the peptide.[14] In many of these cases, the manipulations have now been shown to alter the amyloid assembly pathway and to either promote or deplete the accumulation of intermediates, implicating alternative species in the production of these organismal phenotypes.[2,15]

However, alterations to the assembly pathway could also impact the physical properties of the amyloid that does accumulate and thereby the phenotypic consequences of this process. In this previously unexplored scenario, multiple protein species would contribute to the observed phenotypes, and changes in assembly pathway dynamics would modulate the associated traits by altering the ratios of the contributing species. Here, we experimentally address this possibility for the yeast prion [*PSI*+], the amyloid form of the eukaryotic release factor 3 (eRF3/Sup35).[16–18] In non-prion [*psi*−] cells, Sup35 is soluble and facilitates translation termination, but in prion [*PSI*+] cells, Sup35 is aggregated and functionally compromised, leading to the readthrough of stop codons.[19,20] The severity and toxicity of the [*PSI*+] state were previously thought to reflect the equilibrium between aggregated, non-functional and soluble, functionally engaged Sup35,[21,22] but our studies, presented here, now demonstrate that Sup35 amyloid contributes to the level of translation termination activity in [*PSI*+] cells. The functional contribution of these complexes, however, is impacted by their composition and size, and these amyloid-associated effects are sufficient to explain fluctuations in the prion phenotype.

Results

Aggregated Sup35 Interacts with Its Functional Partners

Loss-of-function mutations in Sup35 phenocopy the translation termination defect observed in a [*PSI*+] strain.[23] However, the existence of gain-of-function beneficial amyloids indicates that amyloid assembly is not incompatible with biochemical activity and raises the possibility that aggregated Sup35 continues to function in its prion conformation. Several previous observations support this hypothesis. First, the Sup35 C-terminal GTPase domain remains accessible on the surface of amyloid fibers *in vitro*.[24,25] Second, Sup35 retains the ability to hydrolyze GTP in its aggregated form *in vitro*.[26] Third, proteins fused to the N-terminal Sup35 prion-determining domain (PrD), such as green fluorescent protein (GFP) and luciferase, retain their activity when incorporated into Sup35 aggregates in [*PSI*+] cells,[19] suggesting that conformational conversion is restricted to the domain required for amyloid formation. Nevertheless, Sup35 must still bind to its functional partner Sup45, the eukaryotic release factor 1 (eRF1), and the ribosome to facilitate translation termination,[27] and its ability to engage in these interactions could be compromised by aggregation.[24]

As a first step toward determining the contribution of aggregated Sup35 to termination activity in a [*PSI*+] strain, we assessed its ability to associate with Sup45 and the ribosome. Previous studies disagree on the whether aggregated Sup35 binds to Sup45[28,29] or not[19,30,31] in [*PSI*+] cells, but in these studies, binding was assessed indirectly by the prion-dependent fractionation of Sup45 to the aggregate-containing pellet following high-speed centrifugation of yeast lysates. A direct assessment of Sup45 association with Sup35 aggregates, however, is complicated by the fact that [*PSI*+] cells contain a mixture of both soluble and aggregated Sup35.[19,20] To circumvent this difficulty, we developed a system to specifically monitor association of functional partners with Sup35 aggregates based on the ability of the PrD to co-aggregate with full-length Sup35.[19,20,32] As expected, the Sup35 PrD, tagged with an HA epitope (PrD-HA), associated with full-length Sup35 in a [*PSI*+] but not a [*psi*−] strain, as assessed by immunocapture (Fig. 1a), demonstrating the ability of this approach to specifically recover aggregated Sup35. Using this PrD-HA system, Sup45 was also specifically co-immunocaptured with PrD-HA from [*PSI*+] but not [*psi*−] lysates (Fig. 1a). Thus, aggregated Sup35 retains its ability to associate with Sup45 in a [*PSI*+] strain.

Ribosomes were also specifically co-immunocaptured with PrD-HA from a [*PSI*+] but not a [*psi*−] lysate, as assessed by RT-PCR of rRNA (Fig. 1b), suggesting an association with aggregated Sup35 as well. Because ribosomes are in excess to Sup35 *in vivo*,[33,34] we performed additional experiments to confirm the specificity of this interaction. Notably, PrD-HA immunocapture was unable to recover ribosomes in a strain whose only functional source of Sup35 activity was the Sup35 catalytic domain (Sup35-C), which cannot interact with prion aggregates (Fig. 1b, lane 6).[32] However, PrD-HA immunocapture recovered ribosomes in the presence of full-length Sup35 (Fig. 1b, compare lanes 4 and 7 with lane 6). Because full-length Sup35 binds to PrD-HA only in a [*PSI*+] strain (Fig. 1a), the dependence of the PrD-HA/ribosome interaction on this protein indicates that prion aggregates interact with ribosomes. As a further test of this interaction, we examined the dependence of the PrD-HA/ribosome interaction on full-length Sup35 through biochemical fractionation on

sucrose gradients. Under these conditions, Sup35 fractionated to the top of the gradient from [*psi⁻*] lysates and to intermediate fractions from [*PSI⁺*] lysates (Fig. 1c). These migration patterns were not perturbed by RNase treatment (Fig. 1c), which destroyed rRNA (Supplementary Fig. 1), indicating that they reflect prion-dependent differences in Sup35 assembly rather than ribosome association. In addition to these Sup35 pools, a fraction of Sup35 was also recovered in the pellet from both [*PSI⁺*] and [*psi⁻*] lysates (Fig. 1c). RNase treatment of the lysates led to the loss of pelletable Sup35 (Fig. 1c), suggesting that this fraction reflects ribosome-engaged Sup35. Notably, the PrD alone did not fractionate to the pellet, but it did so in the presence of full-length Sup35 and intact rRNA in a [*PSI⁺*] lysate (Fig. 1c, compare Sup35-C + PrD to Sup35 + PrD). Thus, this pelleted material contains prion aggregates that are likely engaged with ribosomes *in vivo*.

Aggregated Sup35 Functions in Translation Termination

These observations, together, indicate that aggregated Sup35 interacts with its functional partners in [*PSI⁺*] cells. But, do these interactions contribute to translation termination activity in [*PSI⁺*] cells? To begin to answer this question, we first established the relationship between Sup35 abundance and activity *in vivo*. To do so, we expressed Sup35 from a doxycycline-repressible promoter as the sole source of the protein in a [*psi⁻*] strain and assessed stop-codon readthrough using a GST(UGA)DsRedNLS reporter as a function of Sup35 abundance.[35] In this system, Sup35 activity was present in excess, as termination fidelity was maintained until the level of the protein fell to ~40% with increasing concentrations of doxycycline (Fig. 2a). Below this threshold, there was a near linear increase in stop-codon readthrough, consistent with a limitation in the availability of Sup35 (Fig. 2a). In a wildtype [*psi⁻*] strain, Sup35 was fully soluble, and stop-codon readthrough was barely detectible (Fig. 2a). This combination of parameters placed the [*psi⁻*] state directly on the dose-response curve generated for Sup35 activity by doxycycline titration (Fig. 2a). In contrast, only ~10% of Sup35 protein was soluble in a wildtype [*PSI⁺*] strain, which exhibited a nearly 30-fold increase in stop-codon readthrough relative to a wildtype [*psi⁻*] strain (Fig. 2a). However, the level of stop-codon readthrough observed in the [*PSI⁺*] strain was significantly reduced in comparison with the level predicted for ~10% soluble Sup35 by the dose-response curve (Fig. 2a). These findings imply that aggregated Sup35 makes an appreciable contribution to termination activity in a [*PSI⁺*] strain.

If both aggregated and soluble Sup35 do contribute to termination activity, we would expect that depletion of Sup35 would lead to an increase in stop-codon readthrough only when the total functional pool of Sup35 (i.e. both aggregated and soluble forms of the protein) became limiting. However, if only soluble Sup35 contributed to termination activity in [*PSI⁺*] cells, we would predict that depletion of Sup35 would lead directly to an increase in stop-codon readthrough because the level of soluble Sup35 in a [*PSI⁺*] strain is already below the threshold for faithful termination (Fig. 2a). To test this idea, we expressed Sup35 from a doxycycline-repressible promoter as the sole source of the protein in a [*PSI⁺*] strain. As expected, addition of doxycycline led to a decrease in the steady-state level of Sup35 over time (Fig. 2b). Notably, this inhibition of Sup35 synthesis led to a parallel decrease in both the soluble and aggregated pools of Sup35, indicating that the equilibrium between the two forms of the protein was not perturbed (Fig. 2b). Upon depletion of Sup35, stop-codon

readthrough increased beyond the level observed in a [*PSI*$^+$] strain, but an appreciable increase was only observed after 1.5 generations (Fig. 2c). During this time, approximately 50% of Sup35 was depleted (Fig. 2b), which was consistent with the threshold for the increase in stop-codon readthrough that we determined in a [*psi*$^-$] strain (Fig. 2a). Thus, aggregated Sup35 must contribute to termination activity in a [*PSI*$^+$] strain.

As a complementary approach, we also assessed strain viability upon Sup35 depletion, as the activity of this protein is essential.[23] If soluble Sup35 was the only active form of the protein, we would predict viability to be lost earlier following the depletion of Sup35 in a [*PSI*$^+$] strain, which accumulates only ~10% soluble Sup35 at steady state (Fig. 2a), than in a [*psi*$^-$] strain, where Sup35 is fully soluble (Fig. 2a). To test this possibility, we expressed Sup35 from the cell type-specific promoters P$_{MFA1}$ and P$_{MF\alpha1}$ in *MATa* and *MATα* strains, respectively, and mated these strains together to repress new Sup35 synthesis.[35] We then determined the number of generations supported by the existing pool of Sup35 in [*PSI*$^+$] and [*psi*$^-$] strains by microscopy. Using this system, a [*psi*$^-$] strain persisted for an average of seven generations after repression of Sup35 synthesis. Remarkably, the viability of the [*PSI*$^+$] strain was similar (Fig. 2d), consistent with our observations that aggregated protein must contribute to the overall level of Sup35 activity in [*PSI*$^+$] cells (Fig. 2a, c). If this scenario is indeed the case, conditions that reduce the transmission of Sup35 aggregates to daughter cells, such as treatment with a low level of guanidine HCl (GdnHCl),[36,37] should strongly compromise viability of the [*PSI*$^+$] strain by promoting the more rapid depletion of the existing protein. For the [*psi*$^-$] strain, viability was reduced to an average of five generations in the presence of GdnHCl, presumably reflecting the mild toxicity of the treatment (Fig. 2d).[38] However, viability was more severely reduced to an average of 3.5 generations in the [*PSI*$^+$] strain upon GdnHCl treatment, consistent with a role for aggregated protein in the overall level of Sup35 activity in a [*PSI*$^+$] strain.

[*PSI*$^+$] Toxicity Does Not Correlate with Soluble Sup35 Loss

How does this discovery of aggregate-associated activity impact our mechanistic understanding of the [*PSI*$^+$] phenotype? To address this question, we considered prion toxicity. Under normal laboratory growth conditions, some [*PSI*$^+$] isolates are not detrimental to yeast,[39,40] but these isolates become toxic upon overexpression of either the PrD or full-length Sup35.[22,31,41–43] This toxicity has been linked to the availability of either Sup35 or Sup45, respectively.[31] In the case of PrD overexpression, a previous study proposed that toxicity resulted from the depletion of the small soluble pool of full-length Sup35 in a [*PSI*$^+$] strain through its incorporation into aggregates by mass action.[31] However, the creation of new templates to accept this soluble protein is dependent on the activity of the molecular chaperone Hsp104 and its co-chaperones Hsp70 (Ssa1/2) and Sis1, which together fragment larger aggregates into smaller complexes.[1] This limitation, based on chaperone availability, may restrict the predicted shift in equilibrium toward the aggregate state.[44]

To resolve the mechanism of toxicity associated with Sup35 overexpression in a [*PSI*$^+$] strain, we first determined the effect of PrD overexpression on the level of soluble full-length Sup35. Integration of a plasmid expressing the PrD ~1.3-fold (Supplementary Fig. 2)

into a [*PSI*[+]] strain did not reduce the level of soluble full-length Sup35 in comparison with the parent strain (Fig. 3a). To assess the effects of high-copy overexpression of the PrD on the accumulation of soluble Sup35, we constructed a [*PSI*[+]] yeast strain expressing full-length Sup35 from its own promoter and Sup35-C from a doxycycline-repressible promoter. Sup35-C lacks the PrD, is incapable of incorporating into prion aggregates and suppresses the toxicity of overexpressed PrD.[38,39] We then transformed this strain with a PrD-encoding high-copy plasmid, which leads to ~10-fold overexpression of the PrD on medium lacking uracil or ~100-fold overexpression of the PrD on medium lacking leucine.[31] On medium lacking uracil, the levels of soluble full-length Sup35 decreased only ~2-fold relative to a vector control (Fig. 3b). This modest decrease was similar on medium lacking leucine despite the 10-fold increase in Sup35 expression relative to the medium lacking uracil (Fig. 3b). Thus, the equilibrium between soluble and aggregated protein is limited by factors beyond Sup35 concentration.

Exploiting the different effects of these three levels of PrD expression, we next determined the relationship between the availability of soluble, full-length Sup35 and prion phenotypes by assessing stop codon readthrough and toxicity in these strains. For the high-copy condition, doxycycline was added to the growth medium to repress expression of Sup35-C and allow detection of these phenotypes. Although only high-copy PrD expression affected the level of soluble full-length Sup35 (Fig. 3a, b), both single (Fig. 3c) and high-copy (Fig. 3d) overexpression (assessed on medium lacking uracil) of the PrD led to an increase in stop-codon readthrough. In the case of toxicity, growth impairment was only observed with the highest level of PrD overexpression attained in medium lacking leucine (Fig. 3e), although growth on medium lacking either uracil or leucine led to a similar reduction in the accumulation of soluble full-length Sup35 (Fig. 3b). Thus, these observations reveal additional discordance between Sup35 solubility and activity in a [*PSI*[+]] strain and, together with the finding that Sup35 aggregates contribute to the overall level of termination activity in a [*PSI*[+]] strain (Fig. 2a), indicate that previously unanticipated factors contribute to the severity of prion phenotypes.

Sup35 Aggregate Composition and Size Impacts Activity

What molecular events might explain these disconnects between Sup35 solubility and activity? In addition to the modest changes in the accumulation of soluble Sup35 that we observed upon PrD overexpression, increasing the synthesis rate of the prion protein will also increase the size of aggregates, due to the chaperone-limited fragmentation reaction.[44] This increase in aggregate size could also impact the contribution that Sup35 aggregates make to the overall level of translation termination activity in [*PSI*[+]] cells. Our first indication that this hypothesis might be valid was the disparate behavior of PrD expression from that of mild overexpression of full-length Sup35 in a wildtype [*PSI*[+]] strain. Notably, modest (~1.5-fold, Supplementary Fig. 2) overexpression of full-length Sup35 from a doxycycline-repressible promoter did not lead to the increase in stop codon readthrough observed in cells expressing a similar level of the PrD (Fig. 3c). Given the fact that neither condition perturbed the equilibrium between soluble and aggregated full-length Sup35 (Fig. 3a), the most parsimonious interpretation of this observation is that the incorporation of the

PrD into aggregates of full-length Sup35 diminishes their activities by altering their composition.

To further explore the possibility that overexpression of the PrD reduces aggregate activity, we next assessed their ribosome engagement in the presence of high-copy PrD. Lysates from strains expressing different amounts of the PrD, as well as from control strains, were fractionated on sucrose gradients, and the amount of full-length Sup35 in the ribosome-containing pellet was determined. Similar amounts of pelleted Sup35 were observed in lysates regardless of whether these cells overexpressed the PrD by ~10-fold or not (Fig. 4a, -Ura). In contrast, the partitioning of Sup35 to the pellet was reduced ~4-fold when lysates from cells over-expressing the PrD by ~100-fold were analyzed (Fig. 4a, -Leu). Because only the strong over-expression of the PrD is toxic to cells (Fig. 3e), these results indicate that prion toxicity correlates with a depletion of ribosome-engaged, aggregated Sup35.

PrD overexpression, like that of full-length Sup35, is also predicted to increase the size of Sup35 aggregates *in vivo* due to the enzyme limitation of the fragmentation reaction.[44] *In vivo*, Sup35 aggregates are composed of SDS-resistant polymers that assemble together into a larger native complex, which scales with the size of the polymers.[45] With a single extra copy of the PrD expressed from the *SUP35* promoter, the migration of aggregates on semi-denaturing detergent agarose gels, which preserve the core polymers but not native aggregates, was similar to those isolated from a wildtype strain (Supplementary Fig. 3), suggesting that the increase in stop-codon readthrough associated with this level of PrD expression results from a change in aggregate composition rather than size. However, PrD overexpression from the high-copy plasmid had strong effects on Sup35 aggregate size in a [*PSI*+] strain. When PrD overexpression was induced ~10-fold by growth in medium lacking uracil, some SDS-resistant aggregates remained in the range observed in lysates from the vector control strain (Fig. 4b). However, these species were completely depleted in lysates from cells grown in medium lacking leucine in which the PrD is overexpressed by ~100-fold (Fig. 4b) Thus, toxicity correlates with both the depletion of ribosome-engaged Sup35 aggregates and an increase in aggregate size.

To separate the contributions of aggregate composition and size to their activity *in vivo*, we took advantage of the fact that Sup35 assembles into aggregates of different sizes based on its conformation and the state of cellular proteostasis. For example, Sup35 can adopt a spectrum of conformations that lead to distinct phenotypic states, characterized by the level of stop-codon readthrough.[22,46] Conformations associated with a "weak" phenotype assemble into aggregates of higher thermodynamic stability, increased size and decreased transmissibility relative to conformations associated with a "strong" phenotype (Fig. 5a).[21,44,45] Moreover, deletion of the N-terminal acetyltransferase NatA reduces the size of Sup35 aggregates (Fig. 5a) without altering the equilibrium between aggregated and soluble protein through a complex pathway,[47] and these changes result in a reversal of the translation termination defect in [*PSI*+] cells.[47,48] Using this panel of strains expressing a single copy of PrD-HA, we correlated Sup35 aggregate size with translation termination activity and ribosome association.

Taking into account differences in the equilibrium between aggregated and soluble Sup35 using our dose-response curve (Fig. 2a), we observed an inverse correlation between aggregate size and activity in translation termination. For the [PSI^+]$^{\text{Strong}}$ strain, which accumulated Sup35 aggregates of intermediate size (Fig. 5a), we observed an intermediate level of aggregate-associated translation termination activity (Fig. 5b). Relative to the [PSI^+]$^{\text{Strong}}$ strain, the increased Sup35 aggregate size observed in a [PSI^+]$^{\text{Weak}}$ strain correlated with a decrease in aggregate-associated activity, and the decreased Sup35 aggregate size observed in a [PSI^+]$^{\text{Strong}}$ NatA strain correlated with an increase in aggregate-associated activity (Fig. 5b). Following immunocapture of PrD-HA and analysis of rRNA by RT-PCR, we also noted an inverse correlation with size. The intermediate size aggregates isolated from the [PSI^+]$^{\text{Strong}}$ strain captured an intermediate level of ribosomes; the larger aggregates isolated from the [PSI^+]$^{\text{Weak}}$ strain captured a lower level of ribosomes, and the smaller aggregates isolated from the [PSI^+]$^{\text{Strong}}$ NatA strain captured a higher level of ribosomes (Fig. 5c). Thus, beyond changes in aggregate composition, our observations indicate that smaller Sup35 aggregates engage the ribosome more efficiently and contribute more termination activity to the cell than their larger counterparts.

To develop a more quantitative relationship between Sup35 aggregate size and activity, we took advantage of our previously developed mathematical model of prion propagation.[44] Our previous studies accurately captured the [PSI^+]$^{\text{Strong}}$ and [PSI^+]$^{\text{Weak}}$ states, and we used the same model but with a 3-fold increase in the [PSI^+]$^{\text{Strong}}$ fragmentation rate to capture the [PSI^+]$^{\text{Strong}}$ NatA state, which has an increased accumulation of Hsp104.[47] Using these parameters, we numerically generated aggregate size distributions for the three strains (Fig. 6a), and these outputs accurately recapitulate our experimental observations (Fig. 5a). Using these distributions, we explored three models to explain the activity of Sup35 aggregates relative to their size in a [PSI^+] strain: 1) a linear increase in activity with size, 2) no change in activity with size, and 3) a power decrease in activity with size.

We next calculated the least squares solution that most accurately explains the empirically determined aggregate activities (Fig. 5b) and the dose-response curve for the corresponding level of soluble Sup35 present (Fig. 2a) for each of the model formulations. To compare the fits, we calculated the residual sum of the least squares errors for each model and the Akaike Information Criterion (AIC) (Table 1). AIC is a common model selection test, which considers both the agreement of a statistical model to a given data set and the complexity (number of parameters) of the model. When comparing between models, the model with the lowest AIC is preferred. For model 3, we explored a range of powers (β), and selected a solution of 0.276, the minimum of the residual sum of the least squares errors, as the optimum value (Supplementary Fig. 4). [Note, a linear decrease in aggregate activity with size is represented by the condition β = −1.] As expected based on the inverse correlation between aggregate size and activity that we measured empirically (Fig. 5b), the first model (activity increases linearly with size) has the largest residual sum of least squares errors; the second model (no size dependence of activity) has an intermediate residual sum of least squares errors, and the third model (activity decreases with size) has the lowest residual sum of least squares errors overall (Table 1). By comparing the ratio of the residual sum of least squares errors, model 3 outperforms model 2 by ~27-fold and model 1 by ~578-fold and,

correspondingly, exhibits the lowest AIC of the models (Table 1). Our computational modeling, therefore, reveals an exponential decrease in Sup35 aggregate activity with size (Fig. 6b) as the most robust explanation for the phenotypic variability of these states. This model, in contrast to the others, also uniquely explains the observed threshold effect, in which a 10-fold increase in expression of Sup35 converts a completely benign state into a strictly toxic one (Fig. 3e), by linking a modest change in aggregate size (Fig. 4b, Fig. 5a) to a drastic reduction in activity (Fig. 5b). Thus, amyloid heterogeneity plays an essential role in the determination of protein-only phenotypes.

Discussion

Loss-of-function yeast prion phenotypes are, at first glance, inconsistent with many previous studies that directly analyzed the effects of conformational conversion and assembly on enzymatic activity. For example, diverse proteins, such as GFP, luciferase, carbonic anhydrase III, glutathione-S-transferase (GST), and barnase retain their activities when fused to the PrD of either Sup35[19] or another yeast prion protein Ure2 and aggregated in [*PSI*+] or [*URE3*] strains, respectively,[49] and Ure2 retains its native glutathione peroxidase activity in its fibrillar form.[50] However, these enzymes have either intrinsic activity or act on small diffusible substrates, raising the possibility that the loss-of-function prion phenotypes arise from steric occlusion of essential interactions in the aggregate form.[24,49] Following from this model, the yeast prion [*PSI*+] was previously thought to confer a translation termination defect through sequestration of Sup35 into amyloid aggregates.[19,20] However, our studies reveal that *in vivo* aggregated Sup35, which exhibits the SDS-resistance of *in vitro* amyloid fibers,[51] retains interactions with its functional partners Sup45 and ribosomes (Fig. 1a, b, c), consistent with the exposure of its functional C-terminal domain on the surface of amyloid fibers,[24,25] and contributes termination activity (Fig. 2a, c, d) in [*PSI*+] cells. Thus, the equilibrium between soluble and aggregated Sup35 is insufficient to explain the molecular basis of the [*PSI*+] phenotype *in vivo*.

How does this functional contribution of aggregates impact our understanding of a loss-of-function amyloid phenotype? Within the framework of this refined model, our studies indicate that amyloid aggregates vary in their activities *in vivo* (Fig. 5a, b, 6b), and this heterogeneity provides a molecular explanation for previously enigmatic aspects of prion biology in yeast. First, deletion of the N-terminal acetyltransferase NatA reverses the [*PSI*+] phenotype without altering the accumulation of SDS-resistant Sup35 aggregates.[61,62] Based on our studies, the smaller complexes that accumulate in this strain (Fig. 5a)[47,48] have increased translation termination activity (Fig. 5b) and ribosome association (Fig. 5c), thereby uncoupling Sup35 aggregates from their normal phenotypic effects. Second, benign variants of [*PSI*+] become toxic upon overexpression of the PrD.[22,31,41–43] Based on our observations, this toxicity arises from a decrease in termination activity upon PrD incorporation into aggregates of full-length Sup35 at low doses (Fig. 3c) and/or to a depletion of smaller, ribosome-engaged aggregates at high doses (Fig. 4a, b). Finally, our observations may also provide an explanation for the synthetic lethality of [*PSI*+] with an Hsp104 A503V mutant.[52] While this genetic interaction could reflect a gain-of-function toxicity, expression of Hsp104 A503V in a [*PSI*+] strain increases Sup35 aggregate size, which will decrease the contribution of these complexes to termination activity according to

our observations (Fig. 5b). Consistent with this interpretation, the toxicity of Hsp104 A503V in a [*PSI*+] strain is suppressed by Sup35-C, suggesting it reflects a Sup35 limitation rather than a gain-of-function phenotype.[52] Thus, variation in the composition and size of SDS-resistant Sup35 aggregates, which impact the engagement of these complexes with its functional partners perhaps through changes in their diffusional properties and/or local concentration effects, is a previously unanticipated contributor to the severity and toxicity of the prion state.

In mammals, amyloid toxicity has also been uncoupled from its accumulation in many systems. The general model that has emerged to explain these observations is that intermediates, either on- or off-pathway, that arise during fibrilization are the toxic species.[2,15,53] Significant experimental support for this toxic intermediate model has been collected in mice, *Drosophila*, *C. elegans*, and yeast,[6–14,54] but such a model does not exclude potential contributions of other misfolded species, including amyloid,[55] to cellular dysfunction.[2,53,55,56] Detailed temporal studies using several amyloidogenic proteins have uncovered a multi-step pathway of assembly, in which unstructured oligomeric intermediates arise and progress to more structured protofibrils and ultimately to highly ordered fibers.[2,51] The relative populations of these misfolded species, which are composed of the same protein, are interconnected and, as such, are all impacted by changes in experimental conditions. Each of these misfolded species will present non-native surfaces to the cellular environment[2,56] and may vary in their functional contributions,[57] as we have demonstrated for Sup35 amyloid. Thus, pathogenesis is more likely to reflect the combined effects of this fluctuating population of species, each of which may be associated with a gain and/or loss of function, rather than the appearance of a single toxic species.[2,56]

Beyond uncovering a functional contribution for aggregates *in vivo*, our studies highlight the more nuanced, and often underappreciated, role that amyloid heterogeneity plays in defining protein-based traits. Many amyloidogenic proteins can determine a range of phenotypes *in vivo* upon their aggregation. Especially in the case of prions, this variability is believed to arise from differences in the conformation of the protein,[15,58,59] which impacts the accumulation of the assembled aggregates by altering the rate of their self-replication.[21,44,60] Our studies suggest an alternative and, in some cases, likely interconnected possibility that aggregate size and composition also contribute to the phenotypic variability of protein-based traits. Notably, amyloid size has already been linked to prion transmissibility in mammals and in yeast,[44,60] and factors that influence the severity and toxicity of protein-based traits, such as overexpression of the protein and differences in the accumulation of proteolytic fragments,[2,61] are also likely to alter the physical attributes of aggregates without necessarily changing protein conformation. Thus, amyloid heterogeneity may provide a new window through which protein misfolding disease mechanisms can be viewed.

Methods

Plasmids

All plasmids used in this study are listed in Supplementary Table 1. SB653 is derived from pRS305 and contains the *SUP35* promoter (P_{SUP35}) as an *Eco*RI/*Bam*HI fragment followed by PrD-HA$_3$ as a *Pst*I/*Sal*I fragment subcloned from p316SpSup-HA3-FL.[62] SB782 contains

P_{SUP35}-PrD-HA$_3$ isolated as a *Xho*I/*Sac*I fragment from SB653 and subcloned into the high-copy *leu2-d* plasmid pEMBL-yex.[32] SB736 contains the *CYC1* promoter (P_{CYC1}) as an *Sac*I/*Xba*I fragment and PrD-HA$_3$ as an *BstX*I-*Cla*I fragment in pRS306.[63] SB531 was generated by inserting the *GPD* promoter (P_{GPD}) as a *Sac*I/*Bam*HI fragment, GST-UGA as a *Bam*HI/*Eco*RI fragment and DsRedNLS as a *Eco*RI/*Xho*I fragment into pRS304.[63] SB581 contains a PrD-GFP fusion as a *Bam*HI/*Sac*I fragment and the *SUP35* promoter as an *Eco*RI/*Bam*HI fragment in pRS305.[63] SB397 contains the *SUP35* promoter as a *Eco*RI/*Bam*HI fragment, the PrD as a *Bam*HI/*Sac*II fragment and GFPssrA as a *Sac*II/*Sac*I fragment into pRS306. SB515 contains the *MFα1* promoter ($P_{MFα1}$) as an *Ava*I/*Bam*HI fragment in pFA6a–kanMX4, and SB526 contains the *MFA1* promoter (P_{MFA1}) as a *Bgl*II/*Bam*HI fragment in pFA6a–kanMX6.

Yeast Strains

All strains are derivatives of 74-D694[18] and are listed in Supplementary Table 2. Yeast strains were constructed to ectopically express Sup35, the PrD, or the GST(UGA)DsRedNLS reporter from integrating plasmids (Supplementary Table 1) based on the vectors pRS304, pRS305, or pRS306.[63] These plasmids were integrated following digestion with *Bsu*36I, *Ppu*MI, or *Stu*I, respectively. Protein expression was confirmed by immunoblotting with specific antiserum in all cases. For strains SY2059 and SY2061, the HA$_3$ epitope was fused to the C-terminus of NM-GFP by transformation of a DNA fragment generated by PCR using pFA6a-3HA-kanMX6[64] as a template and primers JP87 and JP88 (Supplementary Table 3). The promoter and the PrD of Sup35 were replaced at the endogenous locus with the *MFA1* promoter by transformation of a PCR fragment generated using SB526 as a template and primers JP8 and 3PMFA1Cterm (Supplementary Table 3). Replacements were selected on complete media supplemented with G418 and confirmed by PCR. The *SUP35* promoter was replaced with P_{tetO7} by transforming strains with a PCR-generated fragment using pCM225[65] as a template and primers TRS218 and TRS219.[66] The *SUP35* promoter was replaced with the *MFα1* promoter by transforming strains with a PCR fragment using SB515 as a template and primers JP33 and JP34 (Supplementary Table 3). The *SUP35* promoter was replaced with the *MFA1* promoter by transforming strains with a PCR fragment using SB526 as a template and primers JP30 and JP8 (Supplementary Table 3). SY2076 was generated by mating SY2070 to 74D-694 [*PSI*$^+$]^{Weak}.[46] SY1170 was generated by mating SY1163 to SY356.[48] SY2061 was generated by mating SY2050 to SY1170. For all matings, tetrads were dissected by micromanipulation on rich medium, and meiotic progeny were characterized for auxotrophies to allow selection of the appropriate strains.

Protein Analysis

Immunocapture was performed as previously described[67] with the following changes: 25 OD$_{600}$ units of cells were harvested in early log phase; lysis buffer contained 10 mM MgCl$_2$; all wash steps were performed at 4°C; lysates were precleared with Protein G Magnetic Beads (New England Biolabs), and immunocapture was performed with anti-HA high affinity rat monoclonal antibody clone 3F10 (Roche Applied Sciences) and Protein G Magnetic Beads (NEB). For RNA isolation, immunocaptured samples were treated with proteinase K at 250 μg/ml in 50 mM Tris-Cl (pH7.4), 50 mM NaCl, 5 mM EDTA, 0.5%

SDS at 42°C for 1 hour. Following proteinase K treatment, phenol:chloroform:isoamyl alcohol (25:24:1) extractions were performed twice followed by ethanol precipitation after the addition of LiCl to 800 mM. Samples were then treated with 4U Turbo DNase (Ambion) for 30 min at 37°C followed by phenol/chloroform extraction and ethanol precipitation with 100 mM sodium acetate, pH 5.2. Samples were resuspended in DEPC-treated water and analyzed by qRT-PCR using SYBR Green One-Step qRT-PCR Kit with ROX (Invitrogen) with 2 mM $MgSO_4$ and primers JP53 and JP54 for 18S rRNA amplification or JP55 and JP56 for 26S rRNA amplification. Dissociation curves generated a single peak for all qPCR reactions. For sucrose gradient fractionation, lysates were prepared by glass-bead disruption at 4°C in lysis buffer [40 mM Tris-HCl (pH 7.4), 150 mM KCl, 15 mM $MgCl_2$, complete protease inhibitor tablet (Roche Applied Sciences) and 20 U/ml rRNAsin (Promega)]; rRNAsin was not included in samples to be treated with RNase. Glass beads were separated, and the lysate was precleared for 3 minutes at $5900 \times g$ at 4°C. 100 μl of the supernatant (200 μg total protein content) was loaded to the top of a 2 ml, 15–60% sucrose gradient made in lysis buffer and centrifuged for 3 hours at 31,000 rpm in a TLS55 swinging bucket rotor using an Optima Max Ultracentrifuge (Beckman). Gradients were separated into thirteen equal fractions by pipetting from the top of each gradient, and the pellet was collected. Samples were analyzed by quantitative immunoblotting with the appropriate antisera using standard protocols. Samples digested with RNase were incubated with 0.5 μg RNase (Roche) for 15 minutes at room temperature immediately prior to loading on the sucrose gradient. RNA visualization was performed by mixing 29 μl of each fraction to generate a 7% sucrose, 0.045% Orange G and 1% SDS solution. 15 μl of this mix was separated on 0.8 % TAE agarose gel with 0.5 μg/ml ethidium bromide. Soluble Sup35 fractions were determined by comparing the level of Sup35 entering an SDS-PAGE gel by quantitative immunoblotting of lysates treated with 2% SDS at either 53°C or 100°C, as previously described.[48] Stop-codon readthrough was determined by analysis of lysates isolated from strains expressing GST(UGA)DsRedNLS by quantitative immunoblotting for GST. Stop-codon readthrough was determined as the fraction of GST-DsRedNLS expression relative to total GST (GST and GST-DsRedNLS). The level of stop codon readthrough attributed to Sup35 aggregates was determined by quantifying the level of soluble Sup35 in the strain by SDS sensitivity as described above, determining the amount of stop codon readthrough expected for that level of soluble protein based on the dose-response curve in Fig. 2a, and subtracting this level of stop codon readthrough from the actual level measured using the reporter GST(UGA)DsRedNLS as described above. Activity was calculated by subtracting the stop codon readthrough attributed to aggregates from unity, and normalizing these levels to the amount of Sup35 in aggregates. For SDD-AGE, cells were grown in liquid YPD, harvested, washed, and mechanically disrupted with glass beads in buffer (50 mM sodium phosphate pH 7.5, 100 mM NaCl, 1mM DTT, 2mM PMSF, and 5 μg/ml Pepstatin). Following clearing of the lysate at $500 \times g$ for 1 minute at 4°C, normalized samples were separated on a 1.5% Tris-glycine agarose gel containing 0.1%SDS, transferred to PVDF membrane, and analyzed by immunoblotting using Sup35-specific antiserum (1:2000 dilution).

Viability Assay

Zygotes were isolated from the indicated crosses by micromanipulation and were allow to divide at 30°C until growth ceased. The resulting microcolonies were disrupted using a micromanipulator and individual cells were counted. Generations were extrapolated by calculating the log base 2 of the number of cells.

Mathematical Modeling

Aggregate distributions were computed for the three prion strains using a stochastic simulation model previously presented.[44] Parameter values for the [*PSI*+]Strong and [*PSI*+]Weak strains were as previously reported.[44] Parameters for the NatA strain were the same for [*PSI*+]Strong except the value for fragmentation was increased 3-fold to account for the elevation of Hsp104.[47] The associated level of aggregate activity was determined for each strain by first determining the level of activity for the soluble fraction of Sup35. The activity associated with Sup35 for [*psi*−] strains (Fig. 2a) was fit using Mathematica's FindFit function to an exponential distribution (a exp(b), a = 4.33777, b = 4.98471). Thus for each simulation, the activity related to the soluble Sup35 was computed using the exponential approximation, and the level of activity attributed to an aggregate was determined using three models: (1) all aggregates have equal activity ($A = \sum_i \alpha_2 n_i$), where A represents aggregate-associated activity, i represents the number of monomers in an aggregate, and n_i represents the number of aggregates of size i), (2) the activity of an aggregate is proportional to the number of monomers ($A = \sum_i \alpha_1 i\, n_i$) (3) the activity of an aggregate is proportional to a power (β) of the number of monomers ($A = \sum_i \alpha_3 i^\beta n_i$). In all cases, α represents a proportionality constant between aggregate activity and size distribution. A least squares fit was used to determine the best fitting parameters for each model. Errors in our observations were assumed to be normally distributed with mean zero and the same variance. As such, the Akaike Information Criterion (AIC) values for each model could be determined with the residual sum of squared errors. In these cases AIC = n log(RSS/n) + 2k + C where RSS is the residual sum of squares, n is the number of data points, k is the number of parameters in the model and C is a constant, which does not contribute to the comparison between models.[68]

Supplementary Material

Refer to Web version on PubMed Central for supplementary material.

Acknowledgements

References

1. Tuite MF, Serio TR. The prion hypothesis: from biological anomaly to basic regulatory mechanism. Nat Rev Mol Cell Biol. 2010; 11:823–833. [PubMed: 21081963]

2. Chiti F, Dobson CM. Protein misfolding, functional amyloid, and human disease. Annu Rev Biochem. 2006; 75:333–366. [PubMed: 16756495]

3. Fowler DM, Koulov AV, Balch WE, Kelly JW. Functional amyloid--from bacteria to humans. Trends Biochem Sci. 2007; 32:217–224. [PubMed: 17412596]

4. Blanco LP, Evans ML, Smith DR, Badtke MP, Chapman MR. Diversity, biogenesis and function of microbial amyloids. Trends Microbiol. 2012; 20:66–73. [PubMed: 22197327]

5. Si K, Choi YB, White-Grindley E, Majumdar A, Kandel ER. Aplysia CPEB can form prion-like multimers in sensory neurons that contribute to long-term facilitation. Cell. 2010; 140:421–435. [PubMed: 20144764]

6. Klement IA, et al. Ataxin-1 nuclear localization and aggregation: role in polyglutamine-induced disease in SCA1 transgenic mice. Cell. 1998; 95:41–53. [PubMed: 9778246]

7. Saudou F, Finkbeiner S, Devys D, Greenberg ME. Huntingtin acts in the nucleus to induce apoptosis but death does not correlate with the formation of intranuclear inclusions. Cell. 1998; 95:55–66. [PubMed: 9778247]

8. Nicoll AJ, Collinge J. Preventing prion pathogenicity by targeting the cellular prion protein. Infect Disord Drug Targets. 2009; 9:48–57. [PubMed: 19200015]

9. Radford HE, Mallucci GR. The Role of GPI-anchored PrP(C) in Mediating the Neurotoxic Effect of Scrapie Prions in Neurons. Curr Issues Mol Biol. 2009; 12:119–128. [PubMed: 19767655]

10. Bueler H, et al. High prion and PrPSc levels but delayed onset of disease in scrapie-inoculated mice heterozygous for a disrupted PrP gene. Mol Med. 1994; 1:19–30. [PubMed: 8790598]

11. Warrick JM, et al. Suppression of polyglutamine-mediated neurodegeneration in Drosophila by the molecular chaperone HSP70. Nat Genet. 1999; 23:425–428. [PubMed: 10581028]

12. Kazemi-Esfarjani P, Benzer S. Genetic suppression of polyglutamine toxicity in Drosophila. Science. 2000; 287:1837–1840. [PubMed: 10710314]

13. Arrasate M, Mitra S, Schweitzer ES, Segal MR, Finkbeiner S. Inclusion body formation reduces levels of mutant huntingtin and the risk of neuronal death. Nature. 2004; 431:805–810. [PubMed: 15483602]

14. Cohen E, Bieschke J, Perciavalle RM, Kelly JW, Dillin A. Opposing activities protect against age-onset proteotoxicity. Science. 2006; 313:1604–1610. [PubMed: 16902091]

15. Collinge J, Clarke AR. A general model of prion strains and their pathogenicity. Science. 2007; 318:930–936. [PubMed: 17991853]

16. Cox B. [*PSI*], a cytoplasmic suppressor of super-suppression in yeast. Heredity. 1965; 20:505–521.

17. Wickner RB. [*URE3*] as an altered URE2 protein: evidence for a prion analog in *Saccharomyces cerevisiae* . Science. 1994; 264:566–569. [PubMed: 7909170]

18. Chernoff YO, Lindquist SL, Ono B, Inge-Vechtomov SG, Liebman SW. Role of the chaperone protein Hsp104 in propagation of the yeast prion-like factor [*PSI* +]. Science. 1995; 268:880–884. [PubMed: 7754373]

19. Patino MM, Liu JJ, Glover JR, Lindquist S. Support for the prion hypothesis for inheritance of a phenotypic trait in yeast. Science. 1996; 273:622–626. [PubMed: 8662547]

20. Paushkin SV, Kushnirov VV, Smirnov VN, Ter-Avanesyan MD. Propagation of the yeast prion-like [*PSI* +] determinant is mediated by oligomerization of the SUP35-encoded polypeptide chain release factor. EMBO J. 1996; 15:3127–3134. [PubMed: 8670813]

21. Tanaka M, Collins SR, Toyama BH, Weissman JS. The physical basis of how prion conformations determine strain phenotypes. Nature. 2006; 442:585–589. [PubMed: 16810177]

22. Zhou P, et al. The yeast non-Mendelian factor [*ETA*+] is a variant of [*PSI*+], a prion- like form of release factor eRF3. EMBO J. 1999; 18:1182–1191. [PubMed: 10064585]

23. Serio TR, Lindquist SL. [*PSI* +]: an epigenetic modulator of translation termination efficiency. Annu Rev Cell Dev Biol. 1999; 15:661–703. [PubMed: 10611975]

24. Baxa U, Keller PW, Cheng N, Wall JS, Steven AC. In Sup35p filaments (the [*PSI* +] prion), the globular C-terminal domains are widely offset from the amyloid fibril backbone. Mol Microbiol. 2011; 79:523–532. [PubMed: 21219467]

25. Glover JR, et al. Self-seeded fibers formed by Sup35, the protein determinant of [*PSI* +], a heritable prion-like factor of S. cerevisiae. Cell. 1997; 89:811–819. [PubMed: 9182769]

26. Krzewska J, Tanaka M, Burston SG, Melki R. Biochemical and functional analysis of the assembly of full-length Sup35p and its prion-forming domain. J Biol Chem. 2007; 282:1679–1686. [PubMed: 17121860]

27. Dever TE, Green R. The elongation, termination, and recycling phases of translation in eukaryotes. *Cold Spring Harb Perspect Biol*. 2012; 4:a013706. [PubMed: 22751155]

28. Czaplinski K, et al. The surveillance complex interacts with the translation release factors to enhance termination and degrade aberrant mRNAs. Genes & Development. 1998; 12:1665–1677. [PubMed: 9620853]

29. Paushkin SV, Kushnirov VV, Smirnov VN, Ter-Avanesyan MD. Interaction between yeast Sup45p (eRF1) and Sup35p (eRF3) polypeptide chain release factors: implications for prion-dependent regulation. Mol Cell Biol. 1997; 17:2798–2805. [PubMed: 9111351]

30. Eaglestone SS, Cox BS, Tuite MF. Translation termination efficiency can be regulated in *Saccharomyces cerevisiae* by environmental stress through a prion-mediated mechanism. EMBO J. 1999; 18:1974–1981. [PubMed: 10202160]

31. Vishveshwara N, Bradley ME, Liebman SW. Sequestration of essential proteins causes prion associated toxicity in yeast. Mol Microbiol. 2009; 73:1101–1114. [PubMed: 19682262]

32. Ter-Avanesyan MD, et al. Deletion analysis of the SUP35 gene of the yeast Saccharomyces cerevisiae reveals two non-overlapping functional regions in the encoded protein. Mol Microbiol. 1993; 7:683–692. [PubMed: 8469113]

33. Didichenko SA, Ter-Avanesyan MD, Smirnov VN. Ribosome-bound EF-1 alpha-like protein of yeast *Saccharomyces cerevisiae* . European Journal of Biochemistry. 1991; 198:705–711. [PubMed: 2050148]

34. Wang M, et al. PaxDb, a database of protein abundance averages across all three domains of life. Mol Cell Proteomics. 2012; 11:492–500. [PubMed: 22535208]

35. Satpute-Krishnan P, Serio TR. Prion protein remodelling confers an immediate phenotypic switch. Nature. 2005; 437:262–265. [PubMed: 16148935]

36. Kawai-Noma S, Pack CG, Tsuji T, Kinjo M, Taguchi H. Single mother-daughter pair analysis to clarify the diffusion properties of yeast prion Sup35 in guanidine-HCl-treated [PSI] cells. Genes Cells. 2009

37. Satpute-Krishnan P, Langseth SX, Serio TR. Hsp104-Dependent Remodeling of Prion Complexes Mediates Protein-Only Inheritance. PLoS Biol. 2007; 5:e24. [PubMed: 17253904]

38. Jung G, Jones G, Masison DC. Amino acid residue 184 of yeast Hsp104 chaperone is critical for prion-curing by guanidine, prion propagation, and thermotolerance. Proc Natl Acad Sci U S A. 2002; 99:9936–9941. [PubMed: 12105276]

39. McGlinchey RP, Kryndushkin D, Wickner RB. Suicidal [*PSI* +] is a lethal yeast prion. Proc Natl Acad Sci U S A. 2011; 108:5337–5341. [PubMed: 21402947]

40. Halfmann R, Alberti S, Lindquist S. Prions, protein homeostasis, and phenotypic diversity. Trends Cell Biol. 2010; 20:125–133. [PubMed: 20071174]

41. Chernoff YO, Derkach IL, Inge-Vechtomov SG. Multicopy SUP35 gene induces de-novo appearance of psi-like factors in the yeast *Saccharomyces cerevisiae* . Current Genetics. 1993; 24:268–270. [PubMed: 8221937]

42. Chernoff YO, et al. Dosage-dependent translational suppression in yeast *Saccharomyces cerevisiae* . Yeast. 1992; 8:489–499. [PubMed: 1523883]

43. Dagkesamanskaya AR, Ter-Avanesyan MD. Interaction of the yeast omnipotent suppressors SUP1(SUP45) and SUP2(SUP35) with non-mendelian factors. Genetics. 1991; 128:513–520. [PubMed: 1874413]

44. Derdowski A, Sindi SS, Klaips CL, DiSalvo S, Serio TR. A size threshold limits prion transmission and establishes phenotypic diversity. Science. 2010; 330:680–683. [PubMed: 21030659]

45. Kryndushkin DS, Alexandrov IM, Ter-Avanesyan MD, Kushnirov VV. Yeast [*PSI* +] prion aggregates are formed by small Sup35 polymers fragmented by Hsp104. J Biol Chem. 2003; 278:49636–49643. [PubMed: 14507919]

46. Derkatch IL, Chernoff YO, Kushnirov VV, Inge-Vechtomov SG, Liebman SW. Genesis and variability of [*PSI*] prion factors in Saccharomyces cerevisiae. Genetics. 1996; 144:1375–1386. [PubMed: 8978027]

47. Holmes WM, Manakee B, Gutenkunst R, Serio TR. Loss of N-terminal Acetylation Creates a Unique Phenotype By Modulating Global Protein Folding. submitted.

48. Pezza JA, et al. The NatA acetyltransferase couples Sup35 prion complexes to the [PSI+] phenotype. Mol Biol Cell. 2009; 20:1068–1080. [PubMed: 19073888]

49. Baxa U, Speransky V, Steven AC, Wickner RB. Mechanism of inactivation on prion conversion of the Saccharomyces cerevisiae Ure2 protein. Proc Natl Acad Sci U S A. 2002; 99:5253–5260. [PubMed: 11959975]

50. Bai M, Zhou JM, Perrett S. The yeast prion protein Ure2 shows glutathione peroxidase activity in both native and fibrillar forms. J Biol Chem. 2004; 279:50025–50030. [PubMed: 15371425]

51. Serio TR, et al. Nucleated Conformational Conversion and the Replication of Conformational Information by a Prion Determinant. Science. 2000; 289:1317–1321. [PubMed: 10958771]

52. Gokhale KC, Newnam GP, Sherman MY, Chernoff YO. Modulation of prion-dependent polyglutamine aggregation and toxicity by chaperone proteins in the yeast model. J Biol Chem. 2005; 280:22809–22818. [PubMed: 15824100]

53. Caughey B, Lansbury PT. Protofibrils, pores, fibrils, and neurodegeneration: separating the responsible protein aggregates from the innocent bystanders. Annu Rev Neurosci. 2003; 26:267–298. [PubMed: 12704221]

54. Douglas PM, et al. Chaperone-dependent amyloid assembly protects cells from prion toxicity. Proc Natl Acad Sci U S A. 2008; 105:7206–7211. [PubMed: 18480252]

55. Urbanc B, et al. Neurotoxic effects of thioflavin S-positive amyloid deposits in transgenic mice and Alzheimer's disease. Proc Natl Acad Sci U S A. 2002; 99:13990–13995. [PubMed: 12374847]

56. Williams AJ, Paulson HL. Polyglutamine neurodegeneration: protein misfolding revisited. Trends Neurosci. 2008; 31:521–528. [PubMed: 18778858]

57. Plakoutsi G, et al. Evidence for a mechanism of amyloid formation involving molecular reorganisation within native-like precursor aggregates. J Mol Biol. 2005; 351:910–922. [PubMed: 16024042]

58. Chien P, Weissman JS, DePace AH. Emerging principles of conformation-based prion inheritance. Annu Rev Biochem. 2004; 73:617–656. [PubMed: 15189155]

59. Frost B, Diamond MI. Prion-like mechanisms in neurodegenerative diseases. Nat Rev Neurosci. 2010; 11:155–159. [PubMed: 20029438]

60. Silveira JR, et al. The most infectious prion protein particles. Nature. 2005; 437:257–261. [PubMed: 16148934]

61. Caughey B. Interactions between prion protein isoforms: the kiss of death? Trends Biochem Sci. 2001; 26:235–242. [PubMed: 11295556]

62. DePace AH, Santoso A, Hillner P, Weissman JS. A critical role for amino-terminal glutamine/asparagine repeats in the formation and propagation of a yeast prion. Cell. 1998; 93:1241–1252. [PubMed: 9657156]

63. Sikorski RS, Hieter P. A system of shuttle vectors and yeast host strains designed for efficient manipulation of DNA in Saccharomyces cerevisiae. Genetics. 1989; 122:19–27. [PubMed: 2659436]

64. Longtine MS, et al. Additional modules for versatile and economical PCR-based gene deletion and modification in Saccharomyces cerevisiae. Yeast. 1998; 14:953–961. [PubMed: 9717241]

65. Belli G, Gari E, Aldea M, Herrero E. Functional analysis of yeast essential genes using a promoter-substitution cassette and the tetracycline-regulatable dual expression system. Yeast. 1998; 14:1127–1138. [PubMed: 9778798]

66. DiSalvo S, Derdowski A, Pezza JA, Serio TR. Dominant prion mutants induce curing through pathways that promote chaperone-mediated disaggregation. Nat Struct Mol Biol. 2011; 18:486–492. [PubMed: 21423195]

67. Bagriantsev SN, Gracheva EO, Richmond JE, Liebman SW. Variant-specific [*PSI* +] Infection is Transmitted by Sup35 Polymers within [*PSI* +] Aggregates with Heterogeneous Protein Composition. Mol Biol Cell. 2008

68. Burnham, KP.; Anderson, DR. Model Selection and Multimodel Interference: A Practical Information-Theoretic Approach. Springer-Verlag: 2002.
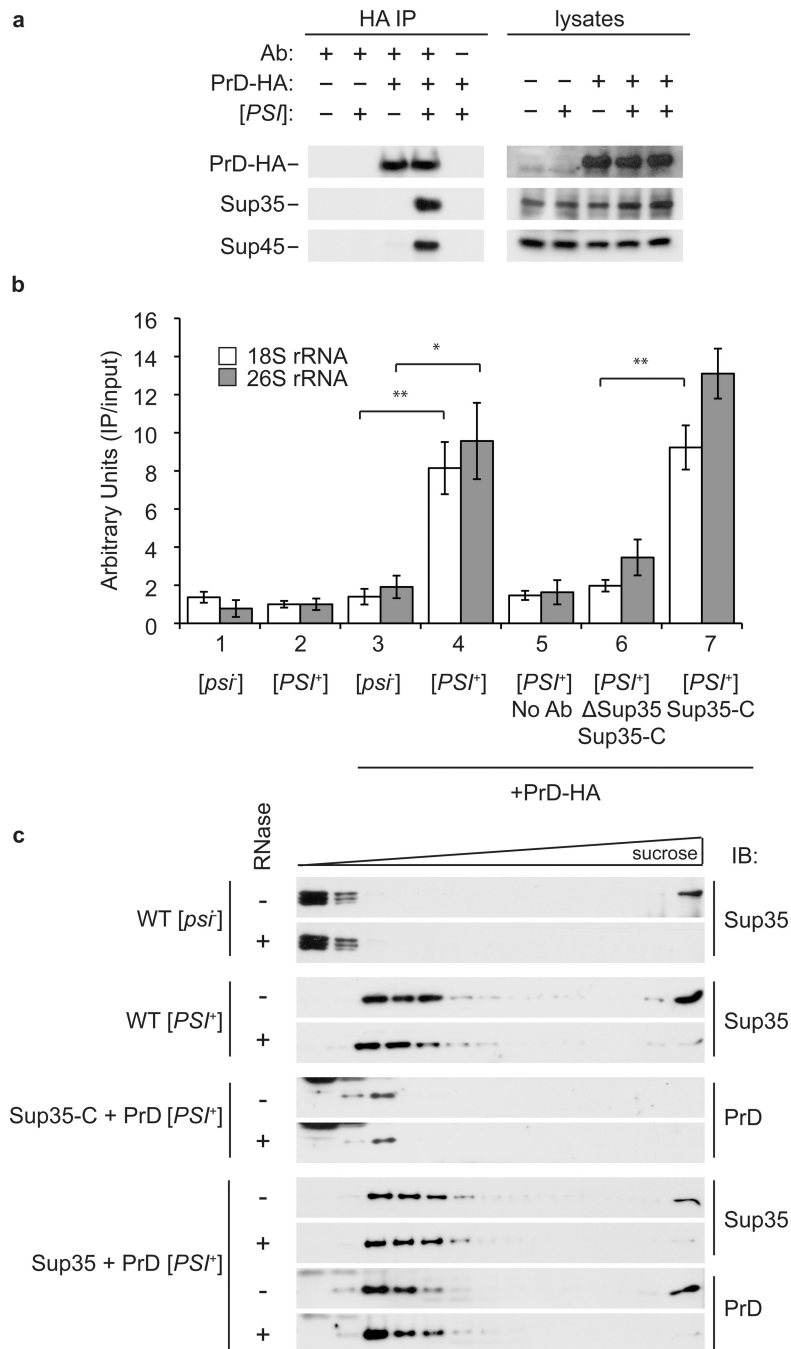
Fig. 1. Aggregated Sup35 associates with Sup45 and the ribosome in [*PSI*⁺] cells

a. PrD-HA expressed in haploid [*PSI*⁺] (+) or [*psi*] (-) yeast strains was immunocaptured (IC) from lysates (Ab, +) in comparison with a reaction lacking specific antiserum (Ab, -), and the isolated complexes were analyzed by SDS-PAGE and immunoblotting for PrD, Sup35 and Sup45. Total protein in the cell lysates was analyzed in parallel to ensure equivalent expression and extraction. **b**. Following PrD-HA IC as in panel (a), the presence of ribosomal subunits was assessed by qRT-PCR using primers specific for either 18S or 26S ribosomal RNAs. All strains express untagged full-length Sup35 except lane 6, which

contains a Sup35 deletion. Lanes 6 and 7 also express the GTPase domain of Sup35 (Sup35-C). The data represent the average of at least three independent experiments, and the error bars represent SEM; *p=0.013; **p 0.004 by unpaired Student's *t*-test. **c**. Sucrose density gradients were used to fractionate lysates isolated from wild-type (WT) [*psi*] or [*PSI*[+]] strains and from [*PSI*[+]] strains expressing the PrD in the presence of Sup35-C or full-length Sup35. The lysates were either untreated (-) or treated with RNase (+) before fractionation. Following centrifugation, fourteen fractions including the pellet were collected and analyzed by immunoblotting (IB) for Sup35 or the PrD.
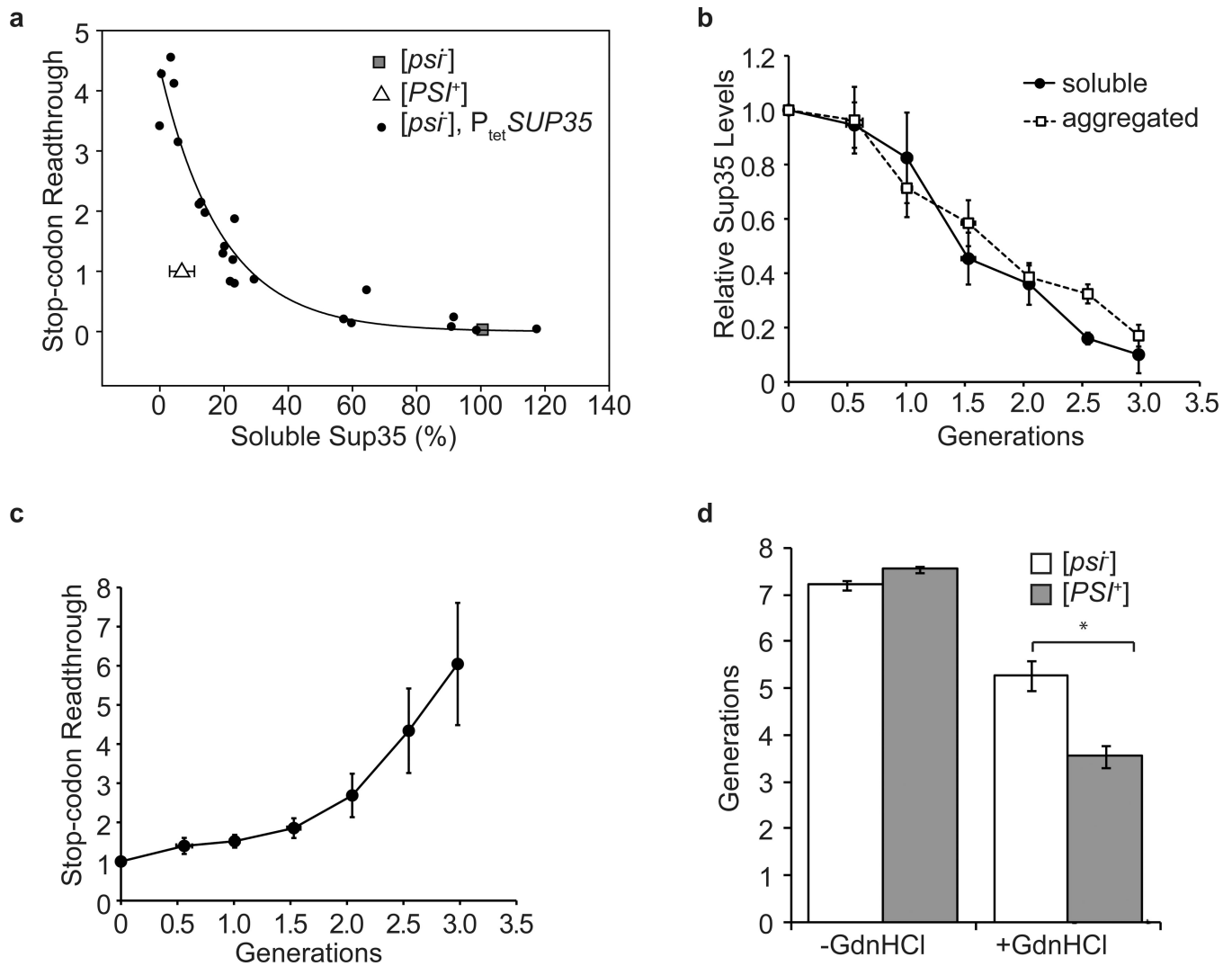
Fig. 2. Aggregated Sup35 Contributes Translation Termination Activity to [*PSI*+] Cells
a. The levels of soluble Sup35 relative to a wildtype [*psi*] strain and stop-codon readthrough relative to wild-type [*PSI*+] strain were determined in lysates from wildtype [*psi*] (gray square), wildtype [*PSI*+] (white triangle) and a [*psi*] strains expressing Sup35 from a doxycycline-repressible promoter (P_{tet}; black circles). These strains also expressed a reporter for stop-codon readthrough (GST(UGA)DsRedNLS). The levels of Sup35 and GST were determined by quantitative immunoblotting. Error bars represent STDEV; n= 6. **b**. The relative levels of soluble (black circles) and aggregated (white squares) Sup35 in a P_{tet}-*SUP35* [*PSI*+] strain were determined at the indicated generations following doxycycline-induced repression of Sup35 synthesis by quantitative immunoblotting. Error bars represent SEM; n=3. **c**. The relative level of stop-codon readthrough of GST(UGA)DsRedNLS a P_{tet}-*SUP35* [*PSI*+] strain was determined by analysis of lysates by quantitative immunoblotting for GST at various times after addition of doxycycline. Error bars represent SEM; n=3. **d**. [*PSI*+] (gray) and [*psi*] (white) zygotes with repressed Sup35 synthesis were analyzed by microscopy to determine the number of generations supported by the existing pool of Sup35

in the absence (-) and presence (+) of guanidine hydrochloride (GdnHCl). Error bars represent SEM; n ⩾ 20; *p=0.0001 by unpaired Student's *t*-test.
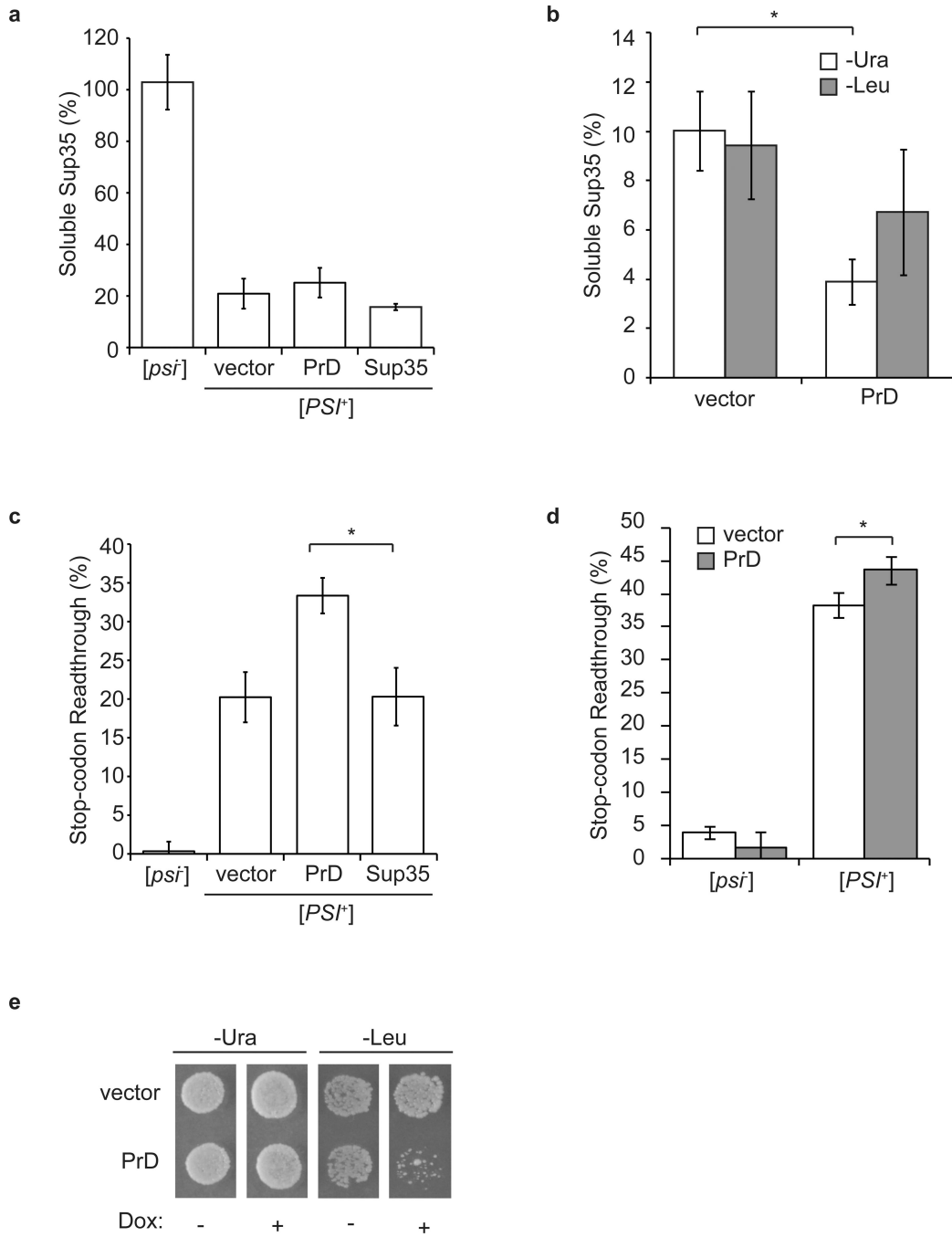
Fig. 3. The severity and toxicity of the [*PSI*+] state cannot be explained by fluctuations in the level of soluble Sup35

a. The levels of soluble Sup35 were determined in lysates from wildtype [*psi*] and [*PSI*+] strains and from [*PSI*+] strains expressing full-length Sup35 from P_{tet} at ~1.5-fold the wildtype level (Sup35) or the PrD from P_{SUP35} (PrD) by quantitative immunoblotting for Sup35. All strains also expressed the stop-codon readthrough reporter GST(UGA)DsRedNLS. Error bars represent SEM; n 3. **b**. Strains expressing full-length Sup35 from P_{SUP35} and Sup35-C from P_{tet} were transformed with either vector or a high-

copy plasmid that over-expresses the PrD ~10-fold on medium lacking uracil (-Ura) or ~100-fold on medium lacking leucine (-Leu). The levels of soluble Sup35 under these conditions were determined in lysates by quantitative immunoblotting. Error bars represent SEM; n 5; *p=0.004 by unpaired Student's *t*-test. **c**. Stop-codon readthrough was determined in lysates from the strains described in panel (a) by quantitative immunoblotting for GST. Error bars represent SEM; n 3; *p=0.017 by unpaired Student's *t*-test.. **d**. Stop-codon readthrough was determined as in panel (c) in lysates from the strains described in panel (b). Strains were grown in medium lacking uracil (-Ura) in the presence of doxycycline to repress expression of Sup35-C. Error bars represent SEM; n 3; *p=0.01 by unpaired Student's *t*-test.. The differences in levels of stop codon readthrough in panels (c) and (d) represent the different baselines in rich (c) and minimal (d) medium. **e**. The strains described in panel (b) were plated on medium lacking uracil (-Ura) or lacking leucine (-Leu) in the absence (-) or presence (+) of doxycycline to repress Sup35-C expression and assess toxicity of overexpressed Sup35.
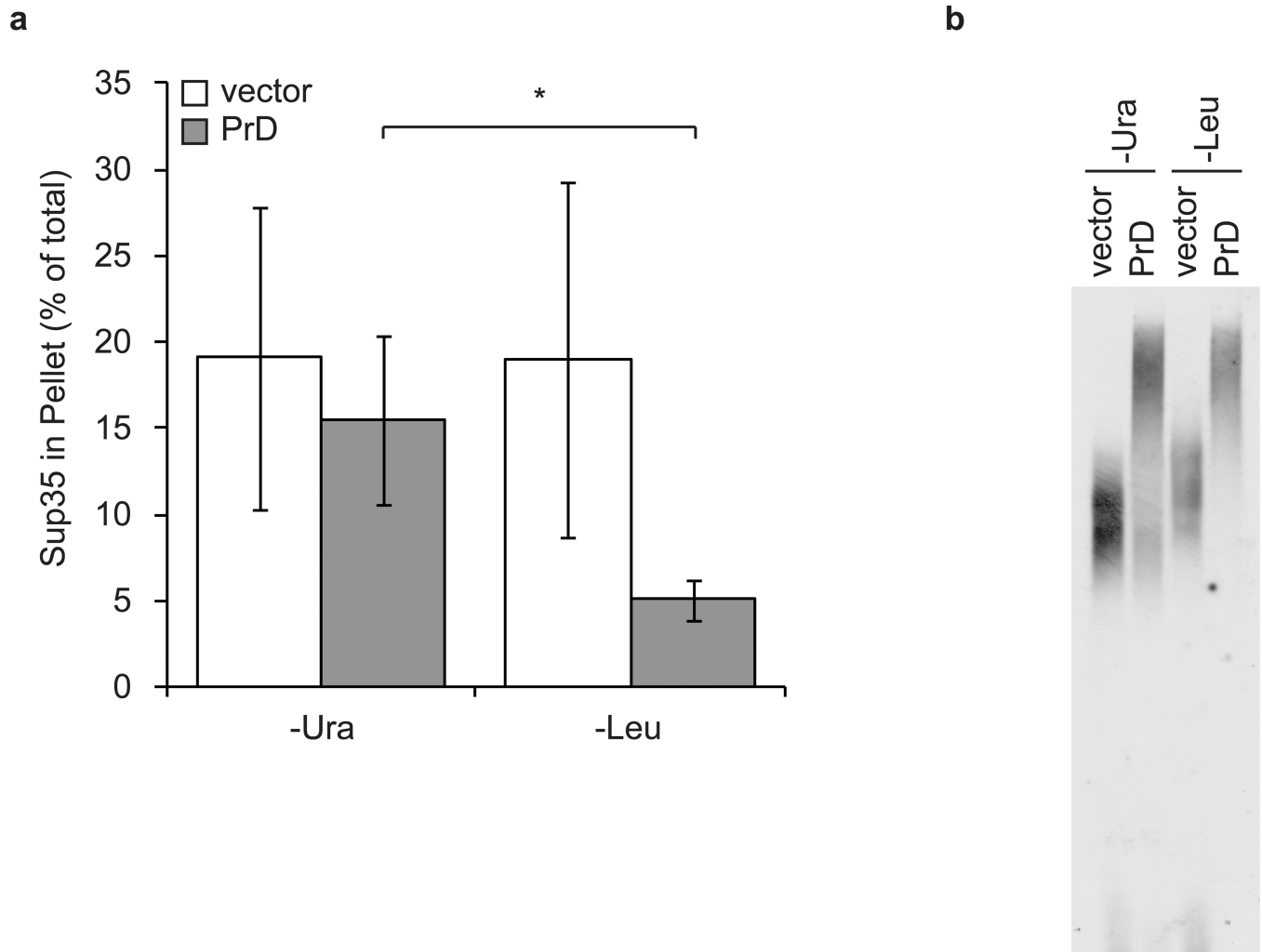
a

b

Fig. 4. The toxicity associated with PrD overexpression correlates with a depletion of a subclass of Sup35 aggregates

a. Lysates from [*PSI*$^+$] strains overexpressing the PrD as described in Fig. 3b that were grown in medium lacking either uracil (-Ura) or leucine (-Leu) were fractionated on sucrose gradients and analyzed by quantitative immunoblotting for Sup35 as described for Fig. 1c. The percentage of Sup35 in the pellet was determined relative to the total amount of Sup35 distributed across the gradient. Error bars represent SEM; n ≥ 5; *p=0.017 by unpaired Student's *t*-test.. **b**. Lysates from strains described in panel (a) were grown in medium lacking uracil (-Ura) or leucine (-Leu) and were analyzed by SDD-AGE and immunoblotting for Sup35. Lysates were normalized for Sup35 expression prior to loading to allow comparisons of aggregate size.
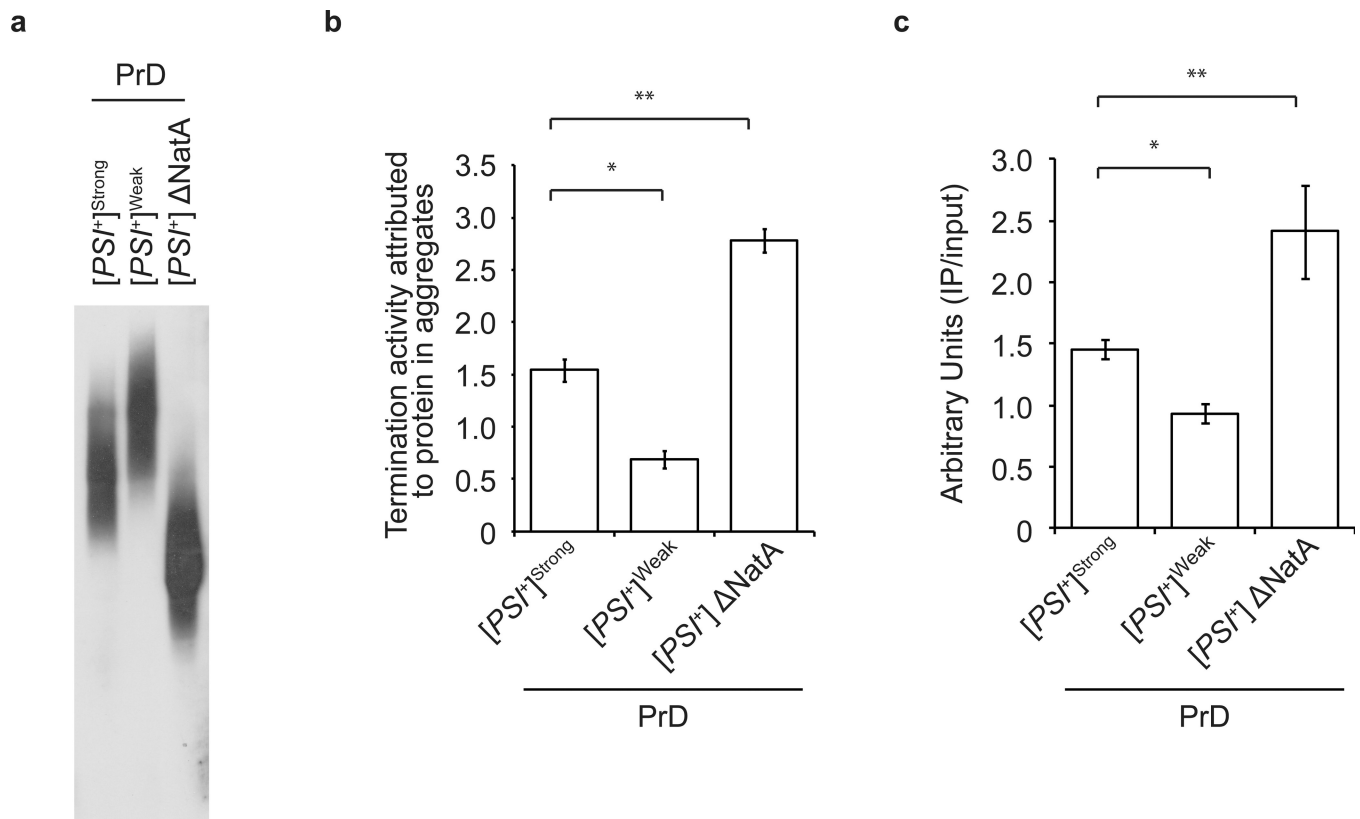
a

PrD

[*PSI*⁺]^Strong [*PSI*⁺]^Weak [*PSI*⁺]ΔNatA

b

c

Fig. 5. Sup35 aggregate size correlates inversely with aggregate activity and association with ribosomes

a. Lysates from [*PSI*⁺]^Strong, [*PSI*⁺]^Weak and [*PSI*⁺] NatA strains, each expressing PrD and GST(UGA)DsRedNLS, were analyzed by SDD-AGE and immunoblotting for Sup35. **b**. Termination activity attributed to aggregates was determined in lysates isolated from the strains described in panel (a) by quantitative immunoblotting for GST. Error bars represent SEM; n=3; *p=0.0031 and **p=0.0012 by unpaired Student's *t*-test. **c**. Lysates isolated from the strains described in panel (a) were immunocaptured as described in Fig. 1b for 18S ribosomal RNA. Error bars represent SEM; n=3; *p =0.001 and **p=0.0004 by unpaired Student's *t*-test.
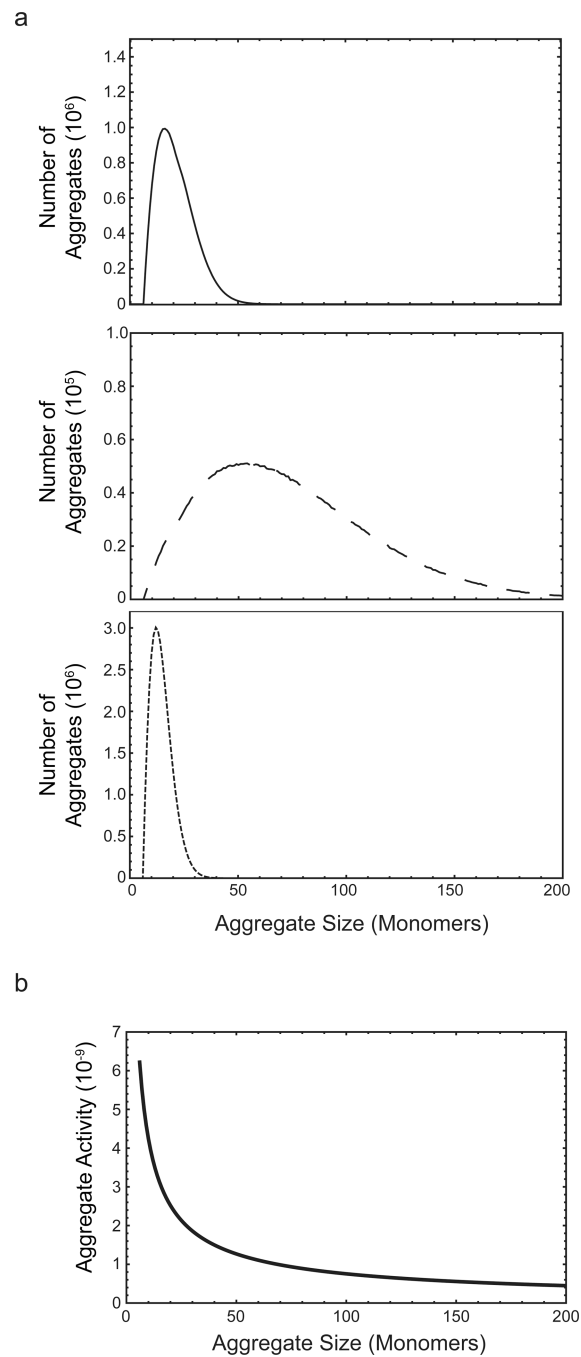
a

b

Fig. 6. Mathematical modeling supports an inverse correlation between Sup35 aggregate size and activity

a. Aggregate size distributions for $[PSI^+]^{\text{Strong}}$ (solid) $[PSI^+]^{\text{Weak}}$ (dashed), and $[PSI^+]$ NatA (dotted) resulting from stochastic simulations of a mathematical model for prion propagation. **b**. The relationship between aggregate activity and size corresponding to model 3 (power decrease in activity with size) for $\beta=0.25$ (see text for details).

Table 1

Analysis of Aggregate-Activity Models

Model	Activity Dependence	RSS*	RSS Ratio (Model X/Model 3)	AIC
1	Linear increase in activity with size	0.446981	578.668617	−3.71155
2	No change in activity with size	0.021168	27.404425	−12.8616
3	Power decrease in activity with size	0.00077243	-	−20.7937

*residual sum of least squared errors